Comproportionation Reaction and Hindered Rotation of Coordinated Pyridine Rings in an Acetate-Bridged Tetraplatinum(II) Cluster with Pyridine-Based Ligands in the Cluster Plane

Tadashi Yamaguchi,*[a] Akira Shibata,[a, b] and Tasuku Ito*[a]

Abstract: A series of pyridine-substituted derivatives of octaacetatotetraplatinum(II), $[Pt_4(CH_3COO)_{8-n}(L)_{2n}]^{n+}$ (L = 4-dimethylaminopyridine (dmap), pyridine (py), 4-cyanopyridine (cpy); $n = 1-4$) were prepared, and the tetra- and octasubstituted forms ($n = 2$ and 4) were isolated. ^{1}H NMR spectra showed that this type of cluster undergoes a comproportionation reaction. Reactions between clusters in which $n = 0$ and 2, $n = 0$ and 4, and $n = 2$ and 4 afforded Pt_4 clusters with $n = 1$, 2, and 3, respectively, as a main product in acetonitrile. The dmap-substituted clusters, *trans*-$[Pt_4(CH_3COO)_6(dmap)_4](ClO_4)_2 \cdot 3CH_3NO_2$ (**3a**$(ClO_4)_2 \cdot 3CH_3NO_2$) and $[Pt_4(CH_3COO)_4(dmap)_8](ClO_4)_4 \cdot 4H_2O$ (**5a**$(ClO_4)_4 \cdot 4H_2O$), have been structurally characterized. Both **3a** and **5a** have a square-planar cluster core comprised of four Pt^{II} ions, and all eight out-of-plane coordination sites are occupied by acetate ligands in a bridging mode. In **5a**, all of the in-plane sites are occupied by dmap ligands. In **3a**, four dmap ligands occupy the coordination sites at the two mutually opposite edges of the square planar cluster skeleton, giving a *trans* tetrasubstituted form of $[Pt_4(CH_3COO)_8]$ (**1**). In octasubstituted **5a**, adjacent dmap ligands are so closely arranged that the Pt–N distances (2.20(3), 2.30(3) Å) are longer than those in tetrasubstituted **3a** (2.13(1), 2.15(1) Å) and related Pt_4 clusters. Furthermore, rotation of the dmap ligand about the Pt–N bond in **5a** was restricted, and the rate constant of the rotation was $4.5\,s^{-1}$ at 20 °C from dynamic NMR study. Cluster $[Pt_4(CH_3COO)_5(dmap)_6]^{3+}$ (**4a**) also exhibited similar hindered rotation with the rate constants of $2.0\,s^{-1}$, $12\,s^{-1}$ and $\approx 10^4\,s^{-1}$ at 20 °C depending on the coordination sites of the dmap ligands in **4a**.

Keywords: cluster compounds · comproportionation · metal–metal interactions · platinum · restricted rotation

Introduction

Octaacetatotetraplatinum(II) $[Pt_4(CH_3COO)_8]$ (**1**) is a well-known Pt^{II} cluster complex with a unique structure[1] and reactivity.[2–4] It has a square-planar cluster core comprised of the four Pt^{II} ions. The coordination geometry around each platinum(II) ion is a distorted octahedron if the Pt–Pt bonds are included.

[a] Dr. T. Yamaguchi, Prof. T. Ito, Dr. A. Shibata
Department of Chemistry, Graduate School of Science
Tohoku University, Sendai 980-8578 (Japan)
Fax: (+81) 22-217-6548
E-mail: yamaguchi@agnus.chem.tohoku.ac.jp
ito@agnus.chem.tohoku.ac.jp

[b] Dr. A. Shibata
Present address: Department of Engineering Science
Niihama National College of Technology (Japan)

Supporting information for this article is available on the WWW under http://www.wiley-vch.de/home/chemistry/or from the author. It contains a) time course of ^{1}H NMR peak intensities during comproportionation; b) temperature dependent ^{1}H NMR spectra of **3′a**; c) Eyring plots for the ring rotation in **4a** and **5a**.

Previously, we reported that the acetate ligands in **1**, which are in the plane of Pt_4 cluster core, are labile, whereas the out-of-plane ligands are inert to substitution.[2] Thus, we prepared some derivatives of the Pt_4 cluster in which all or some in-plane acetates are replaced by bidentate or hexadentate ligands.[4–9] We reported also that **1** undergoes a novel cluster core transformation to Pt_3^{II} clusters with a triangular cluster core when **1** was allowed to react with bulky ligand such as dioximes or *N*,*N*′-dimethylethylendiamine.[10] It was shown that the cluster core transformation was induced by the in-plane ligand substitution of **1**.

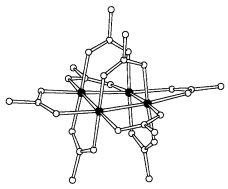

$[Pt_4(CH_3COO)_8]$ (**1**)

In this paper, we report the unprecedented chemistry exhibited by the monodentate ligand (L) substituted derivatives of **1**. Using 4-dimethylaminopyridine (dmap, $pK_a = 9.7$), pyridine (py, $pK_a = 5.2$), and 4-cyanopyridine (cpy, $pK_a = 1.7$), we prepared a series of di-, tetra-, hexa-, and octasubstituted clusters, $[Pt_4(CH_3COO)_{8-n}(L)_{2n}]^{n+}$.

Very interestingly, Pt_4 clusters of this type undergo a comproportionation reaction. The reaction between $[Pt_4(CH_3COO)_{8-n_1}(L)_{2n_1}]^{n_1+}$ and $[Pt_4(CH_3COO)_{8-n_2}(L)_{2n_2}]^{n_2+}$ affords $[Pt_4(CH_3COO)_{8-n_3}(L)_{2n_3}]^{n_3+}$ ($n_3 = (n_1 + n_2)/2$) (see Figure 1 for their structures). The reaction product was, in principle, a single compound with a mean number of coordinated pyridyl ligands and not a mixture of compounds with a statistically distributed number of pyridyl ligands. To our knowledge, such a comproportionation involving ligand scrambling is very rare. In this study, **5a** and **4a** were found to exhibit a novel restricted rotation of the coordinated dmap ligands about the Pt–N bond. Studies thus far reported on hindered rotation about the metal–ligand σ bond in coordination compounds have been limited to complexes with rather large condensed ring ligands.[11] This appears to be the first report involving the hindered rotation of coordinated pyridines that do not have substituent at the 2- and 3-positions.

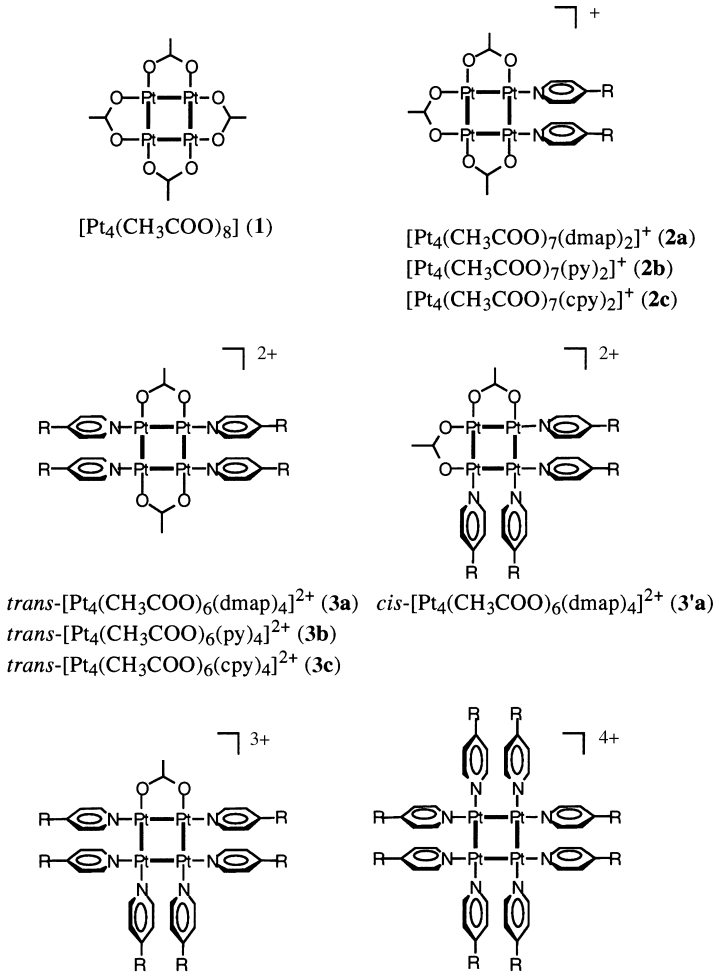

$[Pt_4(CH_3COO)_8]$ (**1**)

$[Pt_4(CH_3COO)_7(dmap)_2]^+$ (**2a**)
$[Pt_4(CH_3COO)_7(py)_2]^+$ (**2b**)
$[Pt_4(CH_3COO)_7(cpy)_2]^+$ (**2c**)

trans-$[Pt_4(CH_3COO)_6(dmap)_4]^{2+}$ (**3a**)
trans-$[Pt_4(CH_3COO)_6(py)_4]^{2+}$ (**3b**)
trans-$[Pt_4(CH_3COO)_6(cpy)_4]^{2+}$ (**3c**)

cis-$[Pt_4(CH_3COO)_6(dmap)_4]^{2+}$ (**3'a**)

$[Pt_4(CH_3COO)_5(dmap)_6]^{3+}$ (**4a**)
$[Pt_4(CH_3COO)_5(py)_6]^{3+}$ (**4b**)
$[Pt_4(CH_3COO)_5(cpy)_6]^{3+}$ (**4c**)

$[Pt_4(CH_3COO)_4(dmap)_8]^{4+}$ (**5a**)
$[Pt_4(CH_3COO)_4(py)_8]^{4+}$ (**5b**)
$[Pt_4(CH_3COO)_4(cpy)_8]^{4+}$ (**5c**)

Figure 1. Pt_4 clusters prepared in this study. Out-of-plane acetates are omitted for clarity.

Results and Discussion

Isolation of tetra- and octasubstituted clusters: Reaction of **1** with pyridines (L = dmap, py, cpy) gives Pt_4 clusters in which the in-plane acetate ligands are replaced by L [Eq. (1), $n = 1-4$]. In this reaction, each acetate ligand is substituted by two monodentate L's, and the degree of substitution increases depending on the amount of added L.

$$[Pt_4(CH_3COO)_8] + 2nL \longrightarrow [Pt_4(CH_3COO)_{8-n}(L)_{2n}]^{n+} + n\,CH_3COO^- \quad (1)$$

The tetrasubstituted, *trans*-$[Pt_4(CH_3COO)_6(L)_4]^{2+}$ (L = dmap (**3a**), py (**3b**), cpy (**3c**)), and octasubstituted, $[Pt_4(CH_3COO)_4(L)_8]^{4+}$ (L = dmap (**5a**), py (**5b**), cpy (**5c**)), clusters were successfully isolated as perchlorate salts [Eq. (1)]. For example, when **1** was allowed to react with four or nine equivalents of dmap and an excess of $NaClO_4$ was added to the resulting solution, precipitates of **3a**$(ClO_4)_2$ or **5a**$(ClO_4)_4$, respectively, were easily obtained. For the less donating ligands (py and cpy), a stoichiometric amount, or excess, of $Ba(ClO_4)_2$ was added to the reaction mixture to remove acetate ligands from **1** as $Ba(CH_3COO)_2$, and use of excess of L was required.

For the tetrasubstituted clusters $[Pt_4(CH_3COO)_6(L)_4]^{2+}$, there are two possible isomers, *trans* (**3**) and *cis* (**3'**), but the reaction depicted in Equation (1) with $n = 2$ afforded exclusively the *trans* isomer (**3**). This probably occurs as a result of the *trans* effect of the pyridyl ligands through the Pt–Pt bond; this has been reported for other Pt_4 clusters of this type.[6–9] In the comproportionation reaction between **1** and $[Pt_4(CH_3COO)_4(dmap)_8]^{4+}$ (**5a**), the formation of a small amount of *cis* isomer in addition to a large amount of *trans* isomer was confirmed (vide infra).

Comproportionation reaction that gives di- and hexasubstituted clusters: In contrast to the tetra- and octasubstituted clusters, the di- and hexasubstituted clusters, $[Pt_4(CH_3COO)_{8-n}(L)_{2n}]^{n+}$ ($n = 1$ and 3; L = dmap, py, cpy), could not be isolated as pure compounds from the reaction in Equation (1). However, they can be produced in an acetonitrile solution as the main component of an equilibrium mixture from the comproportionation reactions between the non- ($n = 0$) and tetrasubstituted ($n = 4$) cluster and between the tetra- ($n = 4$) and octasubstituted ($n = 8$) clusters, respectively [Eqs. (2)–(5)].

$$[Pt_4(CH_3COO)_8] + [Pt_4(CH_3COO)_6(L)_4]^{2+} \underset{k_{-1}}{\overset{k_1}{\rightleftharpoons}} 2\,[Pt_4(CH_3COO)_7(L)_2]^+ \quad (2)$$

$$[Pt_4(CH_3COO)_6(L)_4]^{2+} + [Pt_4(CH_3COO)_4(L)_8]^{4+} \underset{k_{-2}}{\overset{k_2}{\rightleftharpoons}} 2\,[Pt_4(CH_3COO)_5(L)_6]^+ \quad (3)$$

$$K_{c1} = \frac{[\mathbf{2}]^2}{[\mathbf{1}][\mathbf{3}]} = \frac{k_1}{k_{-1}} \quad (4)$$

$$K_{c2} = \frac{[\mathbf{4}]^2}{[\mathbf{3}][\mathbf{5}]} = \frac{k_2}{k_{-2}} \quad (5)$$

Figure 2 shows the ^1H NMR spectral change over time of the comproportionation reaction of an equimolar mixture of **1** and **3a** in CD_3CN at 50 °C. The intensities of the two singlets of **1** (in- and out-of-plane acetate methyls with relative intensity ratio of 1:1) and the three singlets of **3a** (one in-plane

0947-6539/01/0724-5410 $ 17.50+.50/0 *Chem. Eur. J.* **2001**, *7*, No. 24

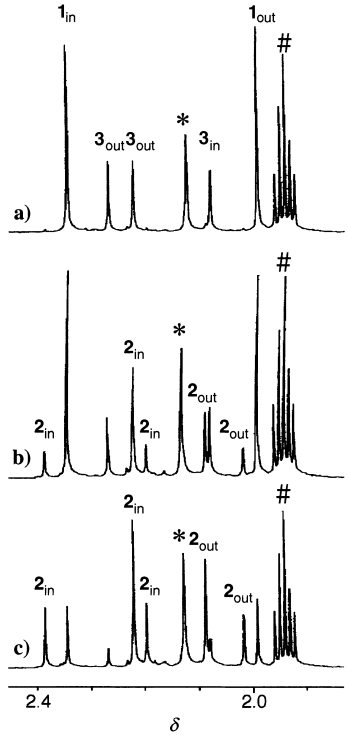

Figure 2. ^{1}H NMR spectral change in the acetate methyl region during the comproportionation reaction between **1** and **3a**: a) 2 h, b) 32 h, and c) 194 h after the reaction initiation. Subscripts, in and out, denote in-plane and out-of-plane acetate, respectively. (#,*:solvent and contaminated water)

and two out-of-plane methyls with intensity ratio of 1:1:1) decreased, and concomitantly the five singlets due to **2a** (two in-plane and three out-of-plane with 1:2:1:1:2) increased with time (see the ^{1}H NMR section and Figure 9 later for assignments). After a week, the reaction reached equilibrium, at which the **2a** to **1** concentration ratio was 6.8:1.0. Although the rate law of the reaction is complicated, it can be simplified when the initial concentrations of both reactants are equal. In fact, the time course of ^{1}H NMR peak intensity of **2a** during the reaction under such conditions was fitted well by assuming the second-order reaction (Figure S1 in the Supporting Information). From the obtained rate constant for the forward reaction (k_1) and the comproportionation constant in Equation (4) ($K_{c1} = k_1/k_{-1}$), which is evaluated from the concentration ratio of the equilibrium mixture, the rate constant of the backward reaction (k_{-1}) was calculated. For the reaction given in Equation (2) between compounds **1** and **3a**, $K_{c1} = 46$, $k_1 = 5.2 \times 10^{-4}\,\text{M}^{-1}\text{s}^{-1}$, and $k_{-1} = 1.1 \times 10^{-5}\,\text{M}^{-1}\text{s}^{-1}$ were obtained. In the same way, comproportionation constants and rate constants for various L's in the reactions given in Equations (2) and (3) were obtained, and they are summarized in Table 1. The comproportionation in Equation (3) involving cpy was not studied because the solubility of **5c** in acetonitrile is very small and the cpy ligand partially dissociates in solution.

Table 1. Rate constants for the comproportionation reactions in Equations (2) and (3).

L	k_1 [$\text{M}^{-1}\text{s}^{-1}$]	k_{-1} [$\text{M}^{-1}\text{s}^{-1}$]	k_2 [$\text{M}^{-1}\text{s}^{-1}$]	k_{-2} [$\text{M}^{-1}\text{s}^{-1}$]	K_{c1}	K_{c2}
dmap	5.2×10^{-4}	1.1×10^{-5}	6.1×10^{-3}	6.8×10^{-5}	46	90
py	5.4×10^{-2}	1.4×10^{-3}	1.8×10^{-1}	4.3×10^{-3}	39	42
cpy	3.0×10^{-1}	1.5×10^{-2}	–[a]	–[a]	20	–[a]

[a] See text.

Both the forward and backward rate constants in the reactions given in Equations (2) and (3) are larger for the comproportionation reactions involving an L with a lower basicity. The fact that the rate constants depend strongly on the kind of pyridyl ligand (three orders of magnitude difference for dmap and cpy) suggests that pyridyl ligand dissociation process contributes largely to the rate constants. A weaker Pt–L bond results in larger rate constants both for the disproportionations and the comproportionations. As discussed later, Pt–N distances in octa- and hexasubstituted clusters are elongated as compared with those in clusters with $n \leq 2$, possibly causing the general trends, $k_1 < k_2$ and $k_{-1} < k_{-2}$. The comproportionation constants are slightly larger for reactions involving an L with a stronger basicity.

Comproportionation reaction between non- and octasubstituted clusters: In a similar way, the reaction between **1** and the octasubstituted cluster **5a** afforded the tetrasubstituted cluster $[Pt_4(CH_3COO)_6(dmap)_4]^{2+}$ (**3a**, **3′a**). Figure 3 shows the ^{1}H NMR spectrum of the equilibrated solution from an equimolar reaction between **1** and **5a** in CD_3CN.

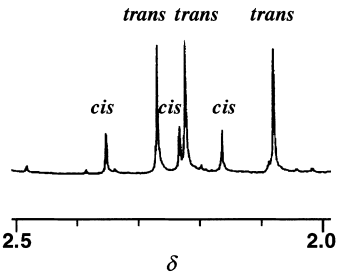

Figure 3. ^{1}H NMR spectrum in the acetate methyl region of an equilibrated solution in the equimolar reaction between **1** and **5a**, showing signals of **3a** (*trans*) and **3′a** (*cis*) (see text).

Interestingly, this reaction proceeded almost to completion, and only trace amounts of the starting compounds **1** and **5a** were detected in the equilibrated solution. Furthermore, both the "*trans*" **3a** and "*cis*" **3′a** isomers were produced with the ratio of 7:3 (Figure 3). As mentioned earlier, the *cis* isomer was not obtained from the reaction between **1** and free dmap [Eq. (1)]. The *trans* effect can be used to explain the appearance of the *cis* isomer. The bold arrows in Scheme 1 show two possible main pathways from the formation of the two isomers, **3a** and **3′a**.

When the disubstituted cluster $[Pt_4(CH_3COO)_7(L)_2]^{2+}$ is formed from **1**, the acetate ligand *trans* to the dmap should be more labile.[12] Thus the *trans* product will be the predominant product. Starting from **5a**, substitution of two dmap ligands by free acetate leads to the formation of the hexasubstituted cluster **4a**. The dmap ligands mutually *trans* to each other should be more labile. Substitution of further pair of dmap ligands by acetate would give the *cis* isomer **3′a**.

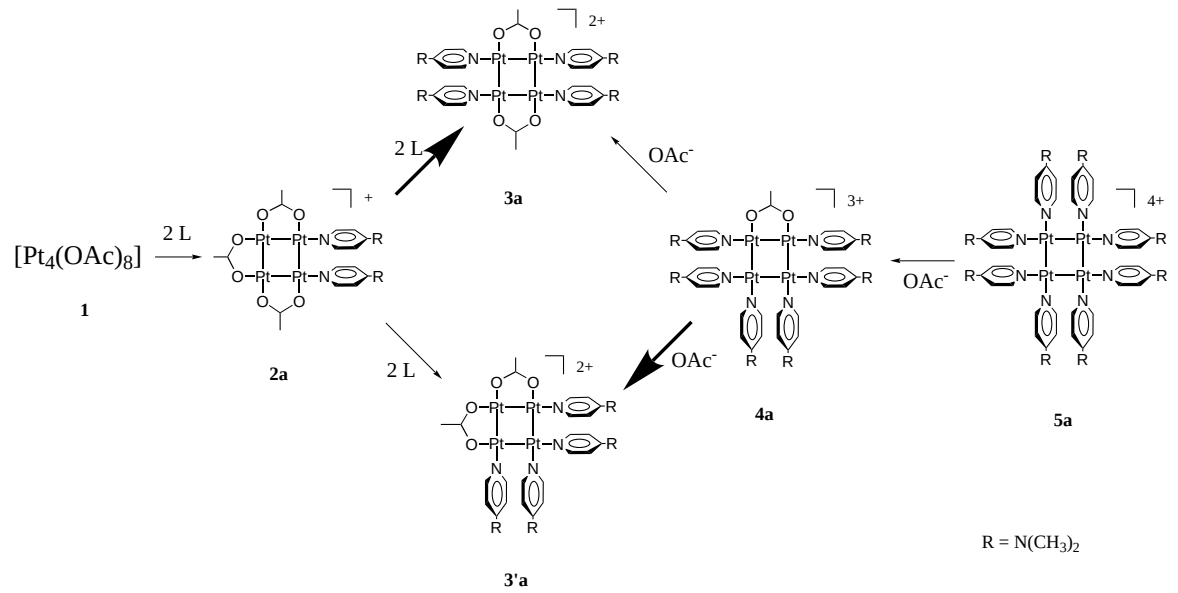

Scheme 1. Reaction pathways for the comproportionation of **1** and **5a**. Out-of-plane acetates are omitted for clarity.

Structures of the tetra- and the octasubstituted clusters with dmap ligands: The crystal structures of *trans*-$[Pt_4(CH_3COO)_6(dmap)_4](ClO_4)_2\cdot 3\,CH_3NO_2$ (**3a**$(ClO_4)_2\cdot 3\,CH_3NO_2$) and $[Pt_4(CH_3COO)_4(dmap)_8](ClO_4)_4\cdot 4H_2O$ (**5a**$(ClO_4)_4\cdot 4\,H_2O$) have been determined by X-ray analyses. Crystallographic and structural determination data are listed in Table 2. An ORTEP drawing of tetrasubstituted cluster **3a** is shown in Figure 4.

The structure of **3a** can be rationalized by comparing it with $[Pt_4(CH_3COO)_8]$ (**1**). Two of the in-plane acetates in **1** have been replaced by four dmap ligands, which occupy coordination sites on the two mutually opposite edges of the square-planar Pt_4 cluster skeleton, giving the tetrasubstituted *trans* form (Figure 1). Four out-of-plane acetates and two in-plane acetates of **1** remain essentially unchanged. There is a crystallographic twofold axis perpendicular to the Pt_4 cluster plane. Selected bond lengths and bond angles are given in Table 3. The Pt–Pt bond *trans* to dmap ligand (Pt1–Pt2 = 2.5299(8) Å) is longer than those in **1** (2.492(1)–2.501(1) Å).[1] This is a consequence of the *trans* influence of the dmap ligand, which has been seen in other Pt_4 clusters with nitrogen donor ligands.[4, 7] The Pt–Pt bond *cis* to the Pt–dmap bond is also elongated (Pt1-Pt2′ = 2.5452(8) Å), but this is due to steric repulsion between adjacent dmap ligands as well as the absence of bridging ligand in the cluster plane. The Pt–N

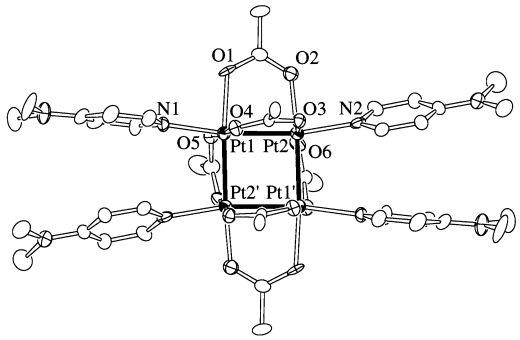

Figure 4. An ORTEP drawing of *trans*-$[Pt_4(CH_3COO)_6(dmap)_4]^{2+}$ (**3a**) in **3a**$(ClO_4)_2\cdot 3\,CH_3NO_2$. Atoms are drawn at the 30 % probability level.

Table 2. Crystallographic data and X-ray experimental conditions for **3a**$(ClO_4)_2\cdot 3\,CH_3NO_2$ and **5a**$(ClO_4)_4\cdot 4\,H_2O$.

	3a$(ClO_4)_2\cdot 3\,CH_3NO_2$	**5a**$(ClO_4)_4\cdot 4\,H_2O$
formula	$Pt_4C_{43}H_{67}N_{11}Cl_2O_{26}$	$Pt_4C_{64}H_{100}N_{16}Cl_4O_{28}$
M_r	2005.28	2463.71
crystal system	monoclinic	tetragonal
space group	$C2/c$ (#15)	$P\bar{4}2_1c$ (#114)
T [K]	293	293
a [Å]	27.361(3)	15.516(2)
b [Å]	13.710(2)	15.516(2)
c [Å]	17.642(2)	20.312(2)
α [°]	90	90
β [°]	107.86(1)	90
γ [°]	90	90
V [Å^3]	6299(1)	14890(1)
λ ($Mo_{K\alpha}$) [Å]	0.71069	0.71069
data collected	7695	4334
independent data [$(F_o) > 3\sigma(F_o)$]	3652	1332
parameters	355	238
R[a]	0.047	0.052
R_w[b]	0.056	0.058

[a] $R = \Sigma(|F_o| - |F_c|)/\Sigma|F_o|$. [b] $R_w = [\Sigma w(|F_o| - |F_c|)^2/\Sigma w|F_o|^2]^{1/2}$.

Table 3. Selected bond lengths [Å] and angles [°] for **3a**$(ClO_4)_2\cdot 3\,CH_3NO_2$ and **5a**$(ClO_4)_4\cdot 4\,H_2O$.

3a$(ClO_4)_2\cdot 3\,CH_3NO_2$				**5a**$(ClO_4)_4\cdot 4\,H_2O$	
Pt1–Pt2	2.5299(8)	Pt1–Pt2	2.5452(8)	Pt1–Pt1′	2.577(2)
Pt1–O1	2.18(1)	Pt1–N1	2.16(1)	Pt1–N1	2.30(2)
Pt2–O2	2.12(1)	Pt2–N2	2.12(1)	Pt1–N2	2.19(3)
Pt1–O4	1.987(8)	Pt1–O5	2.009(9)	Pt1–O1	2.02(2)
Pt2–O3	2.002(9)	Pt2–O6	2.024(9)	Pt1–O2	2.03(2)
Pt2′-Pt1-Pt2	88.44(3)	Pt2-Pt1-O1	86.6(3)	Pt1′-Pt1-Pt1″	88.64(1)
Pt2-Pt1-N1	170.7(3)	Pt2′-Pt1-O1	172.4(3)	Pt1′-Pt1-N1	94.0(7)
Pt2′-Pt1-N1	100.0(4)	O1-Pt1-N1	85.4(4)	Pt1“-Pt1-N1	173.6(7)
Pt1′-Pt2-Pt1	90.92(3)	Pt1-Pt2-O2	85.5(3)	Pt1″-Pt1-N2	94.3(7)
Pt1-Pt2-N2	169.3(4)	Pt1′-Pt2-O2	172.9(3)	Pt1′-Pt1-N2	174.6(7)
Pt1′-Pt2-N2	98.4(4)	O2-Pt2-N2	85.8(5)	N1-Pt1-N2	83(1)

0947-6539/01/0724-5412 $ 17.50+.50/0 *Chem. Eur. J.* **2001**, *7*, No. 24

bond lengths of 2.12(1) and 2.16(1) Å are somewhat longer than those of mononuclear platinum–pyridine complexes;[13] this is ascribed to the *trans* influence of Pt–Pt bond commonly observed in analogous Pt_4 clusters.[4, 6–9] The pyridine rings of the dmap ligands are almost perpendicular to the Pt_4 cluster plane, and two adjacent pyridine rings are not parallel, but are splayed away from each other. The separation between adjacent pyridine nitrogens (N1···N2′ = 3.23(1) Å) is longer than the Pt–Pt distance, and the adjacent amino nitrogens are even further apart (N3···N4′ = 4.46(3) Å). The Pt–O bond lengths of the in-plane acetates are 2.12(1) and 2.18(1) Å, and the average value is comparable to those in **1**. The maximum deviation of the Pt atoms from the Pt_4 best plane is 0.095 Å, which is similar to that in **1** (0.116 Å).[1]

An ORTEP drawing of the octasubstituted cluster **5a** is shown in Figure 5. The structure is described as having all the four of the in-plane acetates in **1** replaced by eight dmap ligands and the four out-of-plane acetates remain unchanged.

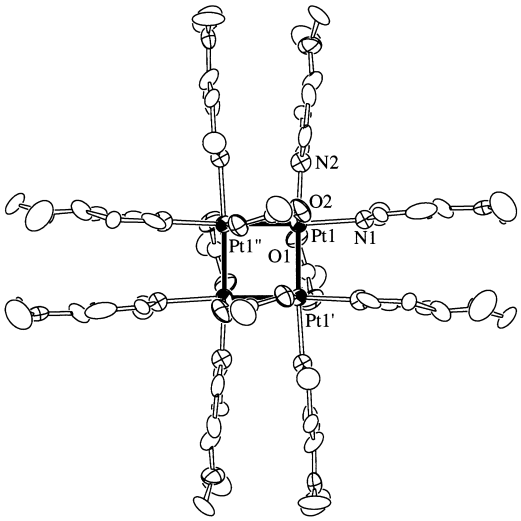

Figure 5. An ORTEP drawing of $[Pt_4(CH_3COO)_4(dmap)_8]^{4+}$ (**5a**) in **5a**$(ClO_4)_4 \cdot 4H_2O$. Atoms are drawn at the 30% probability level.

There is a crystallographic $\bar{4}$ axis at the center of the cluster. Selected bond lengths and bond angles are given in Table 3. The Pt–Pt distance of 2.577(2) Å in **5a** is longer than in **1** and **3a**. This arises from three combined effects: the *trans* influence of the dmap ligand, the absence of in-plane bridging ligands, and the steric repulsion of adjacent two dmap ligands. The Pt–N bond lengths of 2.19(3) and 2.30(3) Å are far longer than those in **3a**. In addition to the *trans* influence of Pt–Pt bond, the steric repulsion between adjacent pyridine rings is again responsible for the elongation. The pyridine rings of dmap are nearly perpendicular to the Pt_4 cluster plane. In contrast to **3a**, the adjacent dmap ligands are nearly parallel. If all dmap ligands are bent toward the outside as in **3a**, the N-Pt-N angle would be smaller than the observed angle of 83(1)° and would cause higher distortion of an octahedral geometry around Pt. The distance between adjacent pyridine nitrogens (N1···N2′ = 2.98(4) Å) is far shorter than that in **3a**. This short contact between two adjacent dmap ligands leads to unprecedented hindered rotation of the pyridine rings discussed below. The maximum deviation of the Pt atoms from the Pt_4 best plane is 0.198 Å in **5a**, which is slightly larger than in **1** and **3a** but similar to the ethylenediamine complex $[Pt_4(CH_3COO)_4(en)_4]^{4+}$ (0.203 Å).[7]

Pyridine ring rotation

*$[Pt_4(CH_3COO)_4(dmap)_8]^{4+}$ (**5a**)*: Even though this compound has D_{2d} symmetry and has only one kind of the dmap ligand, its ^1H NMR spectrum showed two signals with equal intensity for both the α and β pyridine ring protons of the dmap ligand, respectively. Figure 6a shows the temperature-dependent ^1H NMR spectra of **5a** in the β proton region.

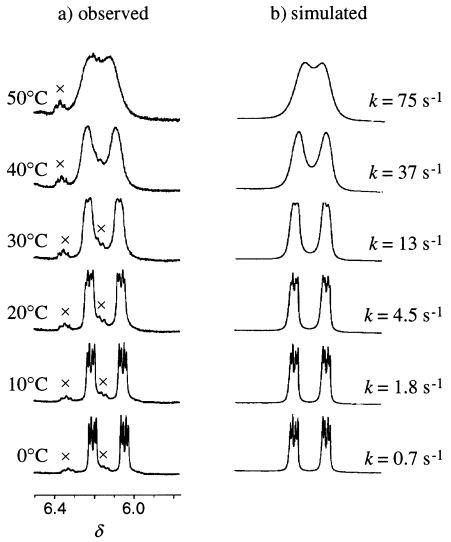

Figure 6. Temperature-dependent ^1H NMR spectra of the dmap β proton in **5a** and the simulated spectra.

Two doublet of doublets with equal intensities at 0°C broaden gradually and coalesce as the temperature rises. This observation is understandable if the rotation of the pyridine rings about the Pt–N bond is restricted. With the restricted rotation, there are two environments for the pyridine ring protons, up (α and β) and down (α* and β*) with respect to the Pt_4 plane, since the arrangement of the out-of-plane acetates exerts different chemical environment on the α, β and α*, β* sites.

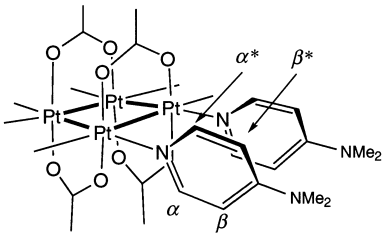

The temperature-dependent ^1H NMR spectra were analyzed by the conventional dynamic NMR method. The simulated spectra are shown in Figure 6b, and the kinetic parameters for the rotational process are listed in Table 4. It is evident that the hindered rotation arises from the stereochemical consequence of the dmap ligands in **5a** as discussed

Table 4. Rotational rate constants and activation parameters for **4a** and **5a** in CD_3CN.

	k [s^{-1}] (at 20 °C)	$\Delta H^{\neq}$ [kJ mol^{-1}]	$\Delta S^{\neq}$ [J mol^{-1} K^{-1}]
5a	4.5	68 ± 2	0 ± 7
4a (site A)[a]	2.0	69 ± 4	-4 ± 12
4a (site B)[a]	12	58 ± 3	-8 ± 11
4a (site C)[a]	ca. 10^4		
3a	$> 10^5$		

[a] See Figure 8.

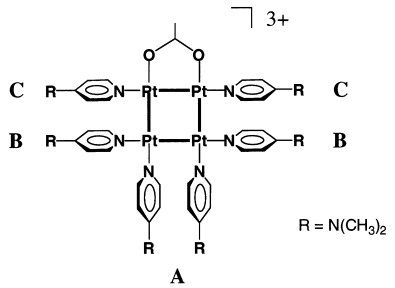

Figure 8. Schematic representation of the three dmap sites in **4a**. Out-of-plane acetates are omitted for clarity.

in the previous section. The very small $\Delta S^{\neq}$ value also supports the restricted rotation of coordinated pyridine ring.

*$[Pt_4(CH_3COO)_5(dmap)_6]^{3+}$ (**4a**)*: Similar temperature-dependent ^{1}H NMR spectra, showing hindered rotation of the coordinated dmap ligands, were also observed for the hexasubstituted cluster **4a**. Three coalescence patterns were observed in temperature-dependent ^{1}H NMR spectra of **4a** (Figure 7), reflecting three chemical environments for the coordinated dmap in **4a** (A, B, and C in Figure 8).

In Figure 7a, the ^{1}H NMR spectra due to the β ring proton of dmap in **4a** are shown. Spectra simulated by dynamic NMR analyses are shown in Figure 7b for sites A and B. A slightly broadened doublet at $\delta = 6.36$ became sharper with an increase in temperature, but remained unchanged above 0 °C; this behavior is similar to the tetrasubstituted cluster **3a** (vide infra). This indicates that rotation at this site is not strongly hindered, and, therefore, the signal is assigned to site C. The two sets of doublet of doublets at $\delta = 6.22$, 6.09 and 6.17, 6.14 are assigned to sites A and B, respectively, because the rotation of the former site is more hindered. Rate constants and activation parameters obtained separately for the three sites are summarized in Table 4. As was expected, the rate constant and activation parameters for site A in **4a** are comparable to those for the dmap rotation in **5a**.

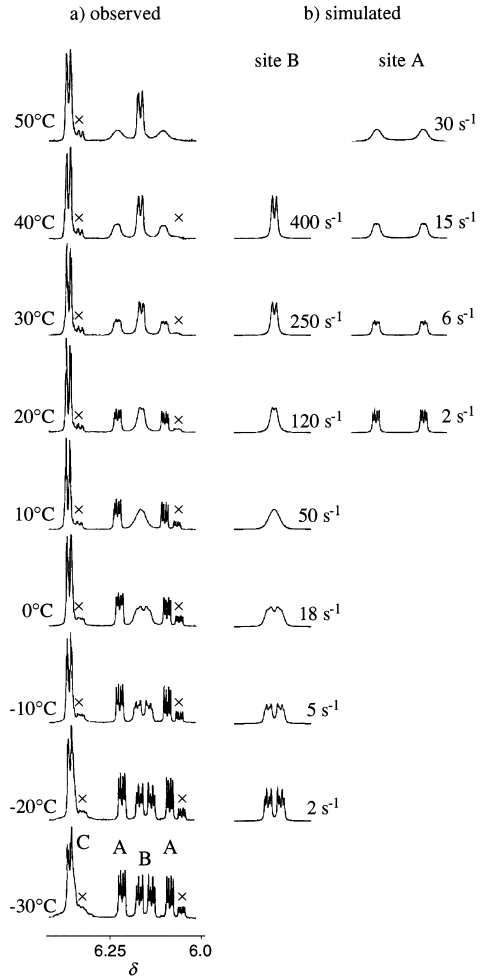

Figure 7. a) Temperature-dependent ^{1}H NMR spectra of the dmap β proton in **4a**. b) Simulated spectra with rate constants. (×: contaminated **3a** and **5a**). See Figure 8 for sites A, B, and C.

*$[Pt_4(CH_3COO)_6(dmap)_4]^{2+}$ (**3a** and **3′a**)*: In contrast to the octa- and hexasubstituted clusters, the ^{1}H NMR spectrum of **3a** at room temperature shows only two doublets corresponding to the α and β pyridine ring protons of the dmap ligand. However, the α proton doublet became broad when the temperature was lowered down to −30 °C. The rotational rate constant was estimated to be $\sim 3 \times 10^4\,s^{-1}$ at −30 °C and $> 10^5\,s^{-1}$ at room temperature by assuming that the chemical shift difference between two environments at slow rotation limit is 1.2 ppm, as is in **5a**. The observations show that the dmap ring in **3a** rotates freely at room temperature, but the rotation is restricted at lower temperature. Ease or difficulty with which **5a** and **3a** undergo the coordinated pyridine rings rotation may be inferred from their X-ray structures. In **3a**, the mutually adjacent dmap ring splay out (see Figure 4), making the rotation easier than in **5a**.

On the other hand, the *cis* isomer **3′a** shows site-dependent rotation of the dmap ligand as does **4a**. In this case, there are two sites similar to sites B and C in Figure 8, and rotation at site C is much faster than at site B. In fact, both characteristics were observed in the temperature-dependent ^{1}H NMR of **3′a** (Figure S2 in the Supporting Information).

^{1}H NMR spectra of $[Pt_4(CH_3COO)_{8-n}(L)_{2n}]^{n+}$: The ^{1}H NMR chemical shifts of the acetate methyl protons in this series of substituted clusters change systematically as a function of the number of pyridyl ligands (n) (Figure 9).

Spectral assignments were easily made by taking into account the systematic chemical shift change with change in n; this can be divided into two series. In one series, the chemical shift increases with an increase in n, while it decreases slightly in the other. The acetate ligands in the Pt_4 cluster plane show

0947-6539/01/0724-5414 $ 17.50+.50/0 *Chem. Eur. J.* **2001**, *7*, No. 24

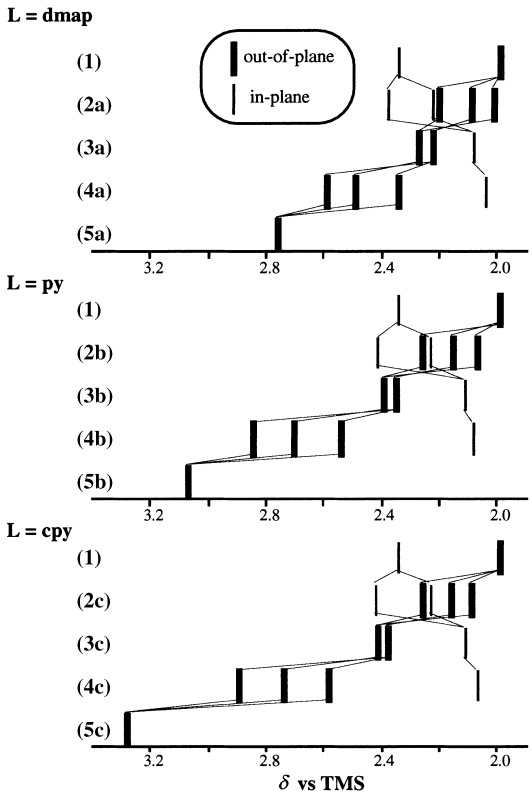

Figure 9. Chemical shifts of the acetate methyl protons in $[Pt_4(CH_3COO)_{8-n}(L)_{2n}]^{n+}$ (L = dmap, py, cpy; $n = 0-4$).

the latter trend, and the out-of-plane acetates the former. The ring current effect of L causes the change in chemical shift, because the pyridyl ligands are coordinated perpendicularly to the Pt_4 cluster plane. The in-plane and out-of-plane acetates are in the shielding and deshielding region, respectively, and the ring current effects increase with an increase in n. The chemical shift of the out-of-plane acetate depends also on the basicity of L. A lower field shift occurs when the pK_a of L is smaller. Thus the out-of-plane acetate signal for **5c** occurs at the lowest field, $\delta = 3.28$, among the present series of clusters.

^{195}Pt NMR spectra: The ^{95}Pt NMR chemical shifts of this series of clusters, $[Pt_4(CH_3COO)_{8-n}(L)_{2n}]^{n+}$, are also dependent on the substitution number (n) and basicity of L. The tetra- and octasubstituted clusters, *trans*-$[Pt_4(CH_3COO)_6(L)_4]^{2+}$ (**3a**–**3c**) and $[Pt_4(CH_3COO)_4(L)_8]^{4+}$ (**5a**, **5b**), showed only one singlet, as expected from their molecular structures. For each type of cluster, the observed peak shifted to higher fields with an increase in the pK_a of L (Table 5).

The di- and hexasubstituted clusters, $[Pt_4(CH_3COO)_7(L)_2]^+$ (**2a**–**2c**) and $[Pt_4(CH_3COO)_5(L)_6]^{3+}$ (**4a**–**4c**), show relatively complicated ^{195}Pt NMR spectra due to the presence of two chemically different Pt atoms (Figure 10), a large Pt–Pt coupling constant, and the presence of isotopomers (natural abundance of ^{195}Pt = 33.8 %). An arrangement of the four Pt atoms in **2a**–**2c** and **4a**–**4c** is of an AA′BB′ type, and, therefore, the ^{195}Pt NMR spectrum of each cluster should be the result of the summation of the resonances for nine isotopomers (A, A_2, B, B_2, AB, AB′, AA′B, ABB′, and AA′BB′) with relative intensity ratios corresponding to their natural abundances. Figure 11a shows the ^{195}Pt NMR spectrum of **2b**, that is, the equilibrated solution of equimolar mixture of **1** and **3b**, which contains two signals due to **1** and **3b** (vide ante).

Table 5. ^{195}Pt NMR chemical shifts and coupling constants (J_{Pt-Pt}) for $[Pt_4(CH_3COO)_{8-n}(L)_{2n}]^{n+}$ (L = dmap, py, cpy; $n = 0-4$).[a]

	δ		J_{Pt-Pt} [Hz]
$[Pt_4(OAc)_7(dmap)_2]^+$ (**2a**)	1113.1	1117.4	[b]
trans-$[Pt_4(OAc)_6(dmap)_4]^{2+}$ (**3a**)	1155.7		–
$[Pt_4(OAc)_5(dmap)_6]^{3+}$ (**4a**)	1055.7	1080.6	6900
$[Pt_4(OAc)_4(dmap)_8]^{4+}$ (**5a**)	989.0		–
$[Pt_4(OAc)_7(py)_2]^+$ (**2b**)	1009.1	1193.5	6440
trans-$[Pt_4(OAc)_6(py)_4]^{2+}$ (**3b**)	1113.5		–
$[Pt_4(OAc)_5(py)_6]^{3+}$ (**4b**)	920.1	1112.2	6760
$[Pt_4(OAc)_4(py)_8]^{4+}$ (**5b**)	919.6		–
$[Pt_4(OAc)_7(cpy)_2]^+$ (**2c**)	933.1	1248.4	6790
trans-$[Pt_4(OAc)_6(cpy)_4]^{2+}$ (**3c**)	1087.2		–
$[Pt_4(OAc)_5(cpy)_6]^{3+}$ (**4c**)	840.6	1154.4	[c]

[a] The chemical shift of **5c** was not obtained due to the low solubility. [b] Not determined due to small difference in chemical shifts of the two sites. [c] Not determined due to the low solubility.

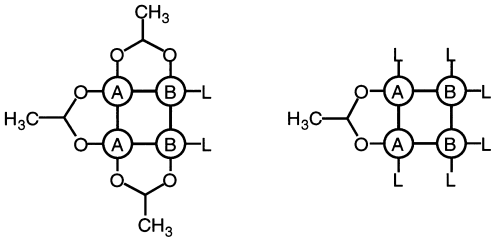

Figure 10. Schematic representation of two Pt sites in **2** (left) and **4** (right). Out-of-plane acetates are omitted for clarity.

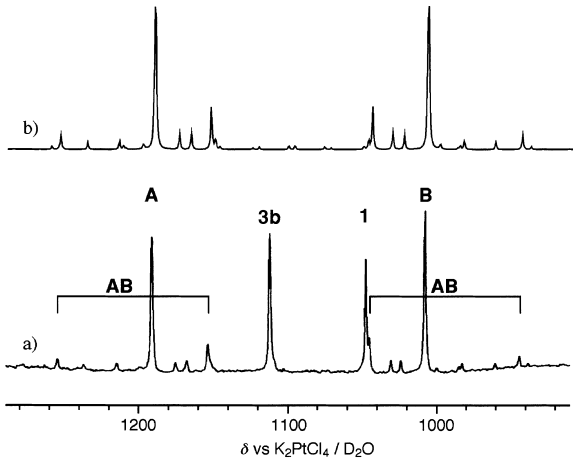

Figure 11. ^{195}Pt NMR spectrum of $[Pt_4(CH_3COO)_7(py)_2]^+$ (**2b**): a) Observed spectrum of an equilibrated solution of **1** and **3b**, which still contains a certain amount of **1** and **3b**. b) Simulated spectrum.

The spectrum was analyzed to obtain chemical shifts and coupling constants, J_{AB}, in the same way as reported previously for $[Pt_4(CH_3COO)_{8-m}(CH_3CONH)_m]$ ($m = 1, 3$)[5] and $[Pt_4(CH_3COO)_4(L\text{-proline})_4]$,[9] both of which have analogous ^{195}Pt NMR patterns. It is evident that two main singlets at $\delta =$ 1009 and 1194 come from two chemically different Pt atoms in

2b, and that an AB quartet can be assigned as shown in Figure 11 ($J_{AB} = 6440$ Hz). Simulation also supports the assignments (Figure 11b).[15] The ^{195}Pt NMR parameters for **2a**–**2c** and **4a**–**4c** were obtained in a similar way (Table 5). Figure 12 shows effects of the pK_a of L on the ^{195}Pt chemical shifts for the series of clusters **2** and **4**.

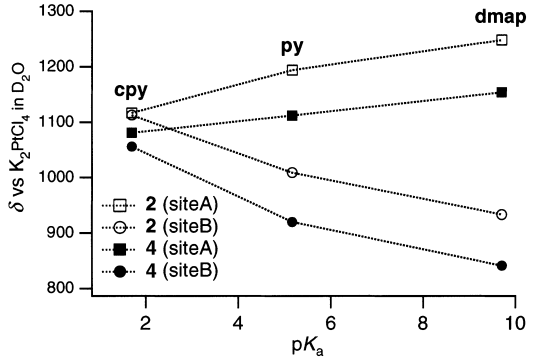

Figure 12. Plots of ^{195}Pt NMR chemical shifts of $[Pt_4(CH_3COO)_{8-n}(L)_{2n}]^{n+}$ (L = dmap, py, cpy; $n = 1,3$) versus pK_a of the coordinated ligand.

For all the clusters in each series, the higher field signal is assigned to site B (the Pt nuclei with more L), and the lower field peak to site A (Figure 10). This assignment was made because the chemical shift of the signal at the higher field depends more strongly on the basicity of L than that at the lower field. In both series **2a**–**2c** and **4a**–**4c**, the signal due to site A nuclei shifts to a lower field and the site B signal shifts to a higher field as the basicity of L becomes lower. It is evident that L affects the chemical shift not only of the Pt bound directly to L (Pt^{direct}), but also Pt *trans* to the Pt–L bond (Pt^{remote}); this is related to the "direct and remote effect" on ^{195}Pt NMR chemical shifts of Pt^{III} dimers with a Pt–Pt bond reported by Appleton et al.[16]

The substitution number (n) also has an effect on the ^{195}Pt chemical shifts for $[Pt_4(CH_3COO)_{8-n}(L)_{2n}]^{n+}$. For clusters with $n = 2$ and 6, averaged chemical shifts between sites A and B, (Figure 10), will be used. Irrespective of L, the chemical shift decreases significantly on going from $n = 4$, to 6 and to 8, while it increases slightly on going from $n = 0$, to 2, and to 4. The remarkable trend observed for the $n = 4$, 6, 8 series can be ascribed to the stereochemical consequence of the coordinated pyridyl ligands. The lengthening of Pt–N bond length found in $[Pt_4(CH_3COO)_4(dmap)_8]^{4+}$ relative to those in $[Pt_4(CH_3COO)_6(dmap)_4]^{2+}$ corresponds to decrease in pK_a of the coordinated dmap ligand in the former.

The Pt–Pt coupling constants (J_{AB}) of the present series of Pt_4 clusters were about 6500 Hz (Table 5), indicating existence of metal–metal bond. Other Pt_4 clusters have similar coupling constants (5500-7700 Hz).[5, 9]

Conclusion

In this study we prepared a series of tetraplatinum cluster complexes with pyridyl ligands $[Pt_4(CH_3COO)_{8-n}(L)_{2n}]^{n+}$ (L = dmap, py, cpy; $n = 1-4$). These clusters undergo a comproportionation reaction with respect to the number of coordinated L. The comproportionation constants for forming the tetrasubstituted clusters ($n = 2$) were quite large, whereas those for di- and hexasubstituted clusters were of the order of 10^1-10^2. The comproportionation rate constants depended strongly on pK_a of pyridyl ligand (L), and decreased three orders of magnitude on going from electron-withdrawing cpy to electron-donating dmap. The octa- and hexasubstituted clusters **5a** and **4a** show the restricted rotation of the coordinated pyridine ring. Such restricted rotations of small aromatic ring about the metal–ligand σ bond have been scarcely reported. As is seen in the X-ray structures of **3a** and **5a**, two dmap ligands are so closely arranged that two ligand planes have to be approximately parallel. Such stereochemistry characteristic of Pt_4 clusters brings about the restricted rotation.

Experimental Section

***trans*-$[Pt_4(CH_3COO)_6(dmap)_4](ClO_4)_2 \cdot H_2O$ (3a$(ClO_4)_2 \cdot H_2O$)**: A solution of dmap (49 mg, 0.4 mmol) in acetonitrile (5 mL) was added to a solution of **1** (125 mg, 0.1 mmol) in acetonitrile (10 mL). After several hours the solution was evaporated using a rotary evaporator. The residue was dissolved in water (2 mL), and a solution of $NaClO_4$ (100 mg) in water (2 mL) was added. An orange precipitate was collected and dissolved in acetonitrile/dichloromethane and hexane was allowed to slowly diffuse into the solution. Yield 100 mg (55%); ^{1}H NMR ($CDCl_3$, TMS): $\delta = 2.08$ (s 6H; OAc-CH_3), 2.22 (s 6H; OAc-CH_3), 2.27 (s, 6H; OAc-CH_3), 3.03 (s, 24H; dmap-CH_3), 6.38 (d, 8H; dmap-*m*), 7.47 (d, 8H; dmap-*o*); ^{195}Pt NMR (CD_3CN, K_2PtCl_4/D_2O): $\delta = 1156$; elemental analysis calcd (%) for $Pt_4C_{40}H_{60}N_8Cl_2O_{21}$ (1840.2): C 26.11, H 3.29, N 6.09; found C 26.06, H 3.09, N 6.09.

$[Pt_4(CH_3COO)_4(dmap)_8](ClO_4)_4 \cdot 4H_2O$ (5a$(ClO_4)_4 \cdot 4H_2O$): A solution of dmap (110 mg, 0.9 mmol) in acetonitrile (5 mL) was added to a solution of **1** (125 mg, 0.1 mmol) in acetonitrile (10 mL). After several hours the solution was evaporated using a rotary evaporator. The residue was dissolved in water (2 mL), and a solution of $NaClO_4$ (100 mg) in water (2 mL) was added. An orange precipitate was collected and recrystallized from acetonitrile/water. Yield 180 mg (73%); ^{1}H NMR (CD_3CN, TMS): $\delta = 2.76$ (s, 12H; OAc-CH_3), 2.90 (s, 48H; dmap-CH_3), 6.05 (dd, 4H; dmap-*m*), 6.22 (dd, 4H; dmap-*m*′), 6.94 (d, 4H; dmap-*o*), 7.60 (d, 4H; dmap-*o*′); ^{195}Pt NMR (CD_3CN, K_2PtCl_4/D_2O): $\delta = 989$; elemental analysis calcd (%) for $Pt_4C_{64}H_{100}N_{16}Cl_4O_{28}$ (2463.8): C 31.20, H 4.09, N 9.10; found: C 31.19, H 3.79, N 8.79.

***trans*-$[Pt_4(CH_3COO)_6(py)_4](ClO_4)_2 \cdot H_2O$ (3b$(ClO_4)_2 \cdot H_2O$)**: A solution of py (50 mg, 0.6 mmol) in acetonitrile (5 mL) was added portion wise to a solution of **1** (125 mg, 0.1 mmol) and $Ba(ClO_4)_2$ (37 mg, 0.11 mmol) in acetonitrile (10 mL), and the mixture was stirred for 1 day. $Ba(CH_3COO)_2$ was filtered off, and the filtrate was evaporated using a rotary evaporator. Acetonitrile (10 mL) and methanol (10 mL) were added to this residue, and the solution was evaporated to give red crystalline solid. This was recrystallized by slow diffusion of hexane into a solution of the residue in acetonitrile/dichloromethane. Yield 80 mg (48%); ^{1}H NMR (CD_3CN, TMS): $\delta = 2.11$ (s 6H; OAc-CH_3), 2.35 (s 6H; OAc-CH_3), 2.39 (s, 6H; OAc-CH_3), 7.39 (t, 8H; py-*m*), 7.92 (t, 4H; py-*p*), 8.06 (d, 8H; py-*o*); ^{195}Pt NMR (CD_3CN, K_2PtCl_4/D_2O): $\delta = 1114$; elemental analysis calcd (%) for $Pt_4C_{32}H_{40}N_4Cl_2O_{21}$ (1668.0): C 23.04, H 2.42, N 3.36; found: C 23.06, H 2.17, N 3.29.

$[Pt_4(CH_3COO)_4(py)_8](ClO_4)_4 \cdot CH_3CN$ (5b$(ClO_4)_4 \cdot CH_3CN$): A solution of py (200 mg, 1.2 mmol) in acetonitrile (5 mL) was added portion-wise to a solution of **1** (125 mg, 0.1 mmol) and $Ba(ClO_4)_2$ (100 mg, 0.3 mmol) in acetonitrile (10 mL), and the mixture was stirred for 1 day. $Ba(CH_3COO)_2$ was filtered off and the filtrate was evaporated to about 2 mL by using a rotary evaporator. After several hours, orange crystalline solids formed. The crude crystals, which contained the hexasubstituted cluster, were dissolved in acetonitrile (25 mL), and $Ba(ClO_4)_2$ (100 mg) and py (1 g)

0947-6539/01/0724-5416 $ 17.50+.50/0 *Chem. Eur. J.* **2001**, *7*, No. 24

were added to this solution. This process was repeated until none of the hexasubstituted cluster remained. The solution was treated in the same way as above to give finally orange crystals. Yield 80 mg (38%); ^{1}H NMR (CD_3CN, TMS): $\delta = 3.07$ (s, 12H; OAc-CH_3), 7.18 (t, 8H; py-*m*), 7.33 (t, 8H; py-*m'*), 7.57 (d, 8H; py-*o*), 8.32 (d, 8H; py-*o'*), 7.72 (t, 8H; py-*p*); ^{195}Pt NMR (CD_3CN, K_2PtCl_4/D_2O): $\delta = 920$; elemental analysis calcd (%) for $Pt_4C_{50}H_{55}N_9Cl_4O_{24}$ (2088.2): C 28.76, H 2.65, N 6.04; found: C 28.81, H 2.67, N 5.86.

***trans*-[$Pt_4(CH_3COO)_6(cpy)_4$](ClO_4)$_2\cdot 2CH_3CN$ ($3c(ClO_4)_2\cdot 2CH_3CN$)**: A solution of cpy (41 mg, 0.4 mmol) in acetonitrile (5 mL) was added by small portions to a solution of **1** (125 mg, 0.1 mmol) and $Ba(ClO_4)_2$ (37 mg, 0.11 mmol) in acetonitrile (10 mL), and the solution was stirred for 1 day. $Ba(CH_3COO)_2$ was filtered off, and the filtrate was evaporated using a rotary evaporator. Acetonitrile (10 mL) and methanol (10 mL) were added to the resulting oil, and the solution was evaporated to give an orange crystalline solid. Yield 90 mg (50%); ^{1}H NMR (CD_3CN, TMS): $\delta = 2.11$ (s 6H; OAc-CH_3), 2.38 (s 6H; OAc-CH_3), 2.41 (s, 6H; OAc-CH_3), 7.80 (d, 8H; cpy), 8.28 (d, 8H; cpy); ^{195}Pt NMR (CD_3CN, K_2PtCl_4/D_2O): $\delta = 1087$; elemental analysis calcd (%) for $Pt_4C_{40}H_{40}N_{10}Cl_2O_{20}$ (1832.1): C 26.22, H 2.20, N 7.05; found: C 26.08, H 2.22, N 6.72.

[$Pt_4(CH_3COO)_4(cpy)_8$](ClO_4)$_4\cdot 5H_2O$ ($5c(ClO_4)_4\cdot 5H_2O$): A solution of cpy (100 mg, 0.95 mmol) in acetonitrile (5 mL) was added by portions to a solution of **3c** (50 mg, 0.03 mmol) and $Ba(ClO_4)_2$ (100 mg, 0.3 mmol) in acetonitrile (10 mL), and the mixture was stirred for 1 day. $Ba(CH_3COO)_2$ was filtered off, and the filtrate was evaporated to about 2 mL by using a rotary evaporator. After several hours, orange crystalline solids formed. The crude crystals, which contained tetra- and hexasubstituted clusters were dissolved in acetonitrile (25 mL), and $Ba(ClO_4)_2$ (200 mg) and cpy (200 mg) were added to this solution. This was carried out until the substitution was complete. The solution was treated in the same way as above to give finally yellow crystals. Yield 20 mg (31%); ^{1}H NMR (CD_3CN, TMS): $\delta = 3.28$ (s, 12H; OAc-CH_3), 8.3–9.0 (br, cpy); elemental analysis calcd (%) for $Pt_4C_{56}H_{54}N_{16}Cl_4O_{29}$ (2337.3): C 28.78, H 2.33, N 9.59; found: C 28.84, H 2.28, N 9.49.

Formation of [$Pt_4(CH_3COO)_7(L)_2$]$^+$ (L = dmap (2a), py (2b), cpy (2c)) in solution: An equimolar mixture of **1** and $[Pt_4(CH_3COO)_6(L)_4]^{2+}$ in CD_3CN (ca. 4 mM) was kept for 2 h at 50 °C; the ^{1}H NMR spectra of the resulting solutions showed the formation of **2**.

Data for ***2a***: ^{1}H NMR (CD_3CN, TMS): $\delta = 2.01$ (s, 3H; OAc-CH_3), 2.09 (s, 6H; OAc-CH_3), 2.20 (s, 3H; OAc-CH_3), 2.22 (s, 3H; OAc-CH_3), 2.38 (s, 3H; OAc-CH_3), 3.02 (s, 12H; dmap), 6.36 (d, 4H; dmap), 7.36 (d, 4H; dmap).

Data for ***2b***: ^{1}H NMR (CD_3CN, TMS): $\delta = 2.07$ (s, 3H; OAc-CH_3), 2.15 (s, 6H; OAc-CH_3), 2.23 (s, 3H; OAc-CH_3), 2.26 (s, 3H; OAc-CH_3), 2.41 (s, 3H; OAc-CH_3), 7.34 (d, 4H; py-*m*), 7.88 (d, 2H; py-*p*), 7.96 (d, 4H; py-*o*).

Data for ***2c***: ^{1}H NMR (CD_3CN, TMS): $\delta = 2.09$ (s, 3H; OAc-CH_3), 2.16 (s, 6H; OAc-CH_3), 2.23 (s, 3H; OAc-CH_3), 2.26 (s, 3H; OAc-CH_3), 2.42 (s, 3H; OAc-CH_3), 7.75 (d, 4H; cpy), 8.20 (d, 4H; cpy).

Formation of [$Pt_4(CH_3COO)_5(L)_6$]$^{3+}$ (L = dmap (4a), py (4b), cpy (4c)) in solution: An equimolar mixture of $[Pt_4(CH_3COO)_6(L)_4]^{2+}$ and $[Pt_4(CH_3COO)_4(L)_8]^{4+}$ in CD_3CN (ca. 4 mM) was kept for 2 h at 50 °C. ^{1}H NMR spectra of the resulting solutions showed formation of **4**.

Data for ***4a***: ^{1}H NMR (CD_3CN, TMS): $\delta = 2.04$ (s, 3H; OAc-CH_3), 2.34 (s, 3H; OAc-CH_3), 2.49 (s, 6H; OAc-CH_3), 2.59 (s, 3H; OAc-CH_3), 2.92 (s, 12H; dmap), 2.93 (s, 12H; dmap), 3.01 (s, 12H; dmap), 6.0–7.6 (br, dmap).

Data for ***4b***: ^{1}H NMR (CD_3CN, TMS): $\delta = 2.08$ (s, 3H; OAc-CH_3), 2.54 (s, 3H; OAc-CH_3), 2.70 (s, 6H; OAc-CH_3), 2.84 (s, 3H; OAc-CH_3), 7.1–8.2 (br, py).

Data for ***4c***: ^{1}H NMR (CD_3CN, TMS): $\delta = 2.07$ (s, 3H; OAc-CH_3), 2.58 (s, 3H; OAc-CH_3), 2.74 (s, 6H; OAc-CH_3), 2.89 (s, 3H; OAc-CH_3), 7.5–8.8 (br, cpy).

X-ray data collection and structure determination: For both **3a**(ClO_4)$_2\cdot$ CH_3NO_2 and **5a**(ClO_4)$_4\cdot 4H_2O$, a suitable crystal coated with epoxy glue was attached to a glass fiber and mounted on a Rigaku AFC7S four-circle diffractometer. The unit cell parameters were obtained by a least-squares refinement of the angular settings of 20 high-angle ($22.58 < 2\theta < 30.08$) reflections. Crystallographic and structural determination data are listed in Table 2. Intensity data in the range $3 < 2\theta < 55°$ were measured by using a $2\theta-\omega$ scan and at a scanning rate of 4.0° min^{-1}. The intensities of three standard reflections did not vary significantly throughout the data collection. Lorentz, polarization, and absorption correction (DIFABS[17]) were applied to the intensity data. All calculations were performed using the teXsan crystallographic software package.[18] Crystallographic data (excluding structure factors) for the structures reported in this paper have been deposited with the Cambridge Crystallographic Data Centre as supplementary publication nos. CCDC-151712 and CCDC-151713. Copies of the data can be obtained free of charge on application to CCDC, 12 Union Road, Cambridge CB21EZ, UK (fax: (+44) 1223-336-033; e-mail: deposit@ccdc.cam.ac.uk).

Data for ***3a***$(ClO_4)_2\cdot 3CH_3NO_2$: A red crystal ($0.35\times 0.20\times 0.06$ mm^3) of **3a**(ClO_4)$_2\cdot 3CH_3NO_2$ recrystallized by diffusion of hexane into a solution of **3a**(ClO_4)$_2$ in $CH_3NO_2/CHCl_3$ was used for data collection. A total of 7695 independent reflections were measured at room temperature. The structure was solved using automatic Patterson analysis method (DIRDIF92 PATTY[19]) and successive difference Fourier syntheses and refined by full-matrix least-squares. The nitromethane molecules were disordered at three sites with 0.5 occupancy each and were refined as rigid body. Anisotropic temperature factors were applied to all non-hydrogen atoms except for the disordered solvent molecule. The final refinement gave $R = 0.048$, and $R_w = 0.057$ for 3652 independent reflections with $[(I_o) > 3\sigma(I_o)]$ and 355 independent parameters.

Data for **5a**(ClO_4)$_4\cdot 4H_2O$: A red crystal ($0.25\times 0.25\times 0.20$ mm^3) of **5a**(ClO_4)$_4\cdot 4H_2O$ recrystallized by slow evaporation of a solution of **5a**(ClO_4)$_4$ in CH_3CN/H_2O was used for data collection. A total of 4334 independent reflections were measured at room temperature. The structure was solved using automatic Patterson analysis method (DIRDIF92 PATTY[19]) and successive difference Fourier syntheses, and refined by full-matrix least-squares. The perchlorate anion was found to be disordered, and one of four oxygen atoms could not be determined and was not included in refinement. Anisotropic temperature factors were applied to all non-hydrogen atoms except for the lattice water. The final refinement gave $R = 0.054$, and $R_w = 0.061$ for 1332 independent reflections with $[(I_o) > 3\sigma(I_o)]$ and 238 independent parameters.

Determination of rotational rate constants of dmap clusters: The rotational rate constants were determined by comparison of observed and simulated spectra. The simulation of the spectrum was performed by DNMR-SIM program.[20] The chemical shifts and coupling constants used in the calculation were taken from the observed spectrum at −30 °C at which the rotation was regarded to be stopped.

Apparatus: ^{1}H and ^{195}Pt NMR spectra were recorded on a JEOL GSX-270 FT-NMR or BRUKER DPX-300 spectrometer. The chemical shifts of ^{195}Pt NMR were referenced to D_2O solution of K_2PtCl_4, using the high-frequency positive-shift sign convention. Variable-temperature ^{1}H NMR were recorded on a BRUKER AM-600 spectrometer. Elemental analyses were carried out at Instrumental Analysis Center, Tohoku University.

Acknowledgements

This work was supported by Grant-in-Aid for Scientific Research (No. 12640531 and Priority Areas No. 10149102 "Metal-assembled Complexes") from the Ministry of Education, Science, Sports, and Culture, Japan.

[1] a) M. A. A. F. de C. T. Carrondo, A. C. Skapski, *J. Chem. Soc. Chem. Commun.* **1976**, 410–411; b) M. A. A. F. de C. T. Carrondo, A. C. Skapski, *Acta Crystallogr. Sect. B* **1978**, *34*, 1857–1862; c) M. A. A. F. de C. T. Carrondo, A. C. Skapski, *Acta Crystallogr. Sect. B* **1978**, *34*, 3576–3578.

[2] T. Yamaguchi, Y. Sasaki, A. Nagasawa, T. Ito, N. Koga, K. Morokuma, *Inorg. Chem.* **1989**, *28*, 4311–4312.

[3] T. Yamaguchi, H. Adachi, Y. Sasaki, T. Ito, *Bull. Chem. Soc. Jpn.* **1994**, *67*, 3116–3118.

[4] A. Shibata, T. Yamaguchi, T. Ito, *Inorg. Chim. Acta* **1997**, *256*, 179–204.

[5] T. Yamaguchi, K. Abe, T. Ito, *Inorg. Chem.* **1994**, *33*, 2689–2691.

[6] T. Yamaguchi, Y. Sasaki, T. Ito, *J. Am. Chem. Soc.* **1990**, *112*, 4038–4040.

[7] T. Yamaguchi, T. Ueno, T. Ito, *Inorg. Chem.* **1993**, *32*, 4996–4997.

  0947-6539/01/0724-5417 $ 17.50+.50/0

[8] T. Yamaguchi, H. Saito, T. Maki, T. Ito, *J. Am. Chem. Soc.* **1999**, *121*, 10738 – 10742.
[9] T. Yamaguchi, A. Shibata, T. Ito, *J. Chem. Soc. Dalton Trans.* **1996**, 4031 – 4032.
[10] a) T. Yamaguchi, N. Nishimura, T.Ito, *J. Am. Chem. Soc.* **1993**, *115*, 1612 – 1613; b) T. Yamaguchi, N. Nishimura, K. Shirakura, T. Ito, *Bull. Chem. Soc. Jpn*. **2000**, *73*, 775 – 784.
[11] E. Alessio, M. Calligaris, M. Iwamoto, L. G. Marzilli, *Inorg. Chem*. **1996**, *35*, 2538 – 2545, and references therein.
[12] The *trans* influence of N-donor ligand through a Pt–Pt bond has been commonly observed in X-ray structures of derivatives of **1**. It has also been shown that substitution of the in-plane acetate of **1** proceeds through an I_d mechanism.
[13] For example, the Pt–N distances in $[Pt(py)_4]^{2+}$ are 2.016 – 2.031 Å: C. H. Wei, B. E. Hingerty, W. R. Busing, *Acta Crystallogr. Sect.C* **1989**, *45*, 26 – 30.
[14] Since the four Pt atoms are in an AA′BB′-type arrangement in **2a** – **2c** and **4a** – **4c**, and the natural abundance of ^{195}Pt is 33.8%, the experimentally observed spectra consists of the summation of spectra due to nine isotopomers (A, A_2, B, B_2, AB, AB′, AA′B, ABB′, and AA′BB′) with relative intensity ratio corresponding to their natural abundances.
[15] The simulation was carried out assuming that $J_{AA'} = J_{BB'} = 6500$ Hz, and the coupling between diagonally opposite platinums, $^2J_{AB'} = 100$ Hz, because they could not be determined accurately from the observed spectrum. The values were estimated taking into consideration J_{AB} for **2b** and $^2J_{Pt-Pt}$ for related compounds.[5]
[16] T. G. Appleton, J. R. Hall, D. W. Neale, *Inorg. Chim. Acta* **1985**, *104*, 19 – 31.
[17] N. Walker, D. Stuart, *Acta Crystallogr. Sect. A* **1983**, *39*, 158 – 166.
[18] teXsan, single-crystal structure analysis software, version 1.7, Molecular Structure Corporation, The Woodlands, TX, **1995**.
[19] P. T. Beurskens, G. Admiraal, W. P. Bosman, S. Garcia-Granda, R. O. Gould, J. M. M. Smits, C. Smykalla, The DIRDIF program system, **1992**.
[20] G. Haegele, R. Fuhler, T. Lenzen, *Comput. Chem*. **1995**, *19*, 277 – 282.

Received: November 7, 2000
Revised: June 19, 2001 [F2853]

  0947-6539/01/0724-5418 $ 17.50+.50/0